◎ 논 문
◎ Original Paper

DOI: https://doi.org/10.5293/kfma.2024.27.2.057
ISSN (Print): 2287-9706

# 펌프수차 비속도에 따른 S-곡선 영역 수력성능 및 내부유동 비교

쉬레스트 우즈왈* · 최영도**†

# Comparison on the Pump Turbine Hydraulic Performance and Internal flow in S-Curve Region by Specific Speed

Ujjwal Shrestha*, Young-Do Choi**†

*Key Words : Pump-Turbine(펌프수차), Performance(성능), S-Curve(S-곡선), Specific speed(비속도), Turbine mode(수차모드), Pump mode(펌프모드)*

## ABSTRACT

The demand for pump turbines is increasing to eradicate the fluctuating, unpredictable, and delocalized energy production from wind and solar. The pump turbine design and the geometrical shape (diameter and width ratios) are based on specific speeds. The pump turbine's specific speed directly influenced hydraulic performance and internal flow behavior. Besides hydraulic performance and internal flow, the pump turbine encounters the S-Curve region when operating at a partial flow rate in turbine mode. The S-Curve region is sensitive to the geometrical shape of the pump turbine. At S-Curve region and partial flow conditions, the high specific speed pump turbine has better flow characteristics than a low specific speed pump turbine.

## 1. Introduction

The promotion of renewable energy is increasing rapidly to reduce carbon emissions. Renewable energy sources like wind and solar have experienced rapid advancement. The demand for energy storage systems has immensely increased due to the enhancement of renewable energy sources like solar and wind. Among the various energy storage systems available, the pump turbine system is the most preferable for a large amount of energy storage, which swiftly switches between modes and assists in balancing intermittent disturbance of renewable sources on the power grid[(1)]. Furthermore, the pump turbine can operate in generation and consumption modes depending upon the electricity demand. Hence, it promotes electricity consumption and economy simultaneously[(2)].

Pump turbines are required to operate in both pump and turbine modes, with opposite flow and rotation. The four quadrants' operational characteristics at specific guide vane openings are observed in the pump turbine. Fig. 1 shows the pump turbine's four quadrant characteristics on the flow speed curve[(3)]. When designing a pump turbine, pump mode performance should be considered because the pump turbine shape is similar to a centrifugal pump rather than the Francis turbine. According to the specific speed, the pump turbine meridional shape is different. The meridional shape of the pump turbine determines its hydraulic performance, cavitation, pressure fluctuations, and S-Curve. The pump turbine instability occurs at low load off-design operating conditions closer to the runaway in turbine mode[(4)]. The S-Curve region occurs when the pump turbine

* Graduate School, Department of Mechanical Engineering, Mokpo National University
** Department of Mechanical Engineering, Institute of New and Renewable Energy Technology Research, Mokpo National University
† 교신저자, E-mail : ydchoi@mnu.ac.kr

operates in turbine mode at partial flow conditions. The S-Curve can be evaluated on unit speed vs. unit discharge characteristics curve. Furthermore, the meridian and circumferential velocity coefficients are advantageous in the S-Curve prediction[5].

Many researchers conducted various studies on the internal flow analysis of the S-Curve of pump turbines. Pejovic et al.[6] analyzed the flow behavior of the pump turbine during the load rejection process. Nicolet et al.[7] performed a numerical analysis to show the unsteady flow behavior in the pump turbine during runaway conditions. Hasmatuchi et al.[8,9] performed experimentation on a low-specific speed pump turbine to understand the flow mechanism under partial flow conditions in turbine mode. Guggenberger et al.[10,11] experimented with the S-Curve region to measure static pressure and visualize flow using PIV. Staubli et al.[12] performed steady and unsteady CFD analysis to understand flow behavior in the S-Curve region. Yin et al.[13] showed that an increase in the meridional flow passage of the medium-specific speed pump turbine makes the S-Curve weaker than the original pump turbine.

Much research has been conducted to explain the flow behavior in the S-Curve characteristics in the pump turbine. The reasonable criterion for the inception of the S-Curve in the pump turbine is still unclear. The various parameters have influenced the S-Curve in the pump turbine when operating at part-load turbine mode. The guide vane opening and impeller geometric parameters (diameter ratio, width ratio, and blade angles) play a significant role in the S-Curve region. Consequently, this paper focuses on the S-Curve behavior according to the pump turbine's specific speed. Furthermore, the impeller geometry is directly related to the specific speed. The motive of the study is to understand and generalize the S-Curve nature according to the pump turbine's specific speed.

## 2. Design and Methodology

### 2.1 Design of pump turbine model

The pump turbine model is used for performance investigation and internal flow analysis. The specific speeds of the pump turbine in pump and turbine modes are calculated using Eqs. (1) and (2), respectively.

$$N_S = \frac{N\sqrt{Q_P}}{H_P^{0.75}} \tag{1}$$

$$N_{S_T} = \frac{N\sqrt{P_T}}{H_T^{1.25}} \tag{2}$$

where $N_S$ and $N_{ST}$ are the specific speeds of the pump turbine in pump mode and turbine mode, respectively. $N$, $Q$, $H$, and $P$ are rotational speed ($min^{-1}$), flow rate ($m^3/s$), effective head (m), and output power (kW). The subscript $P$ and $T$ represent the pump and turbine modes, respectively.

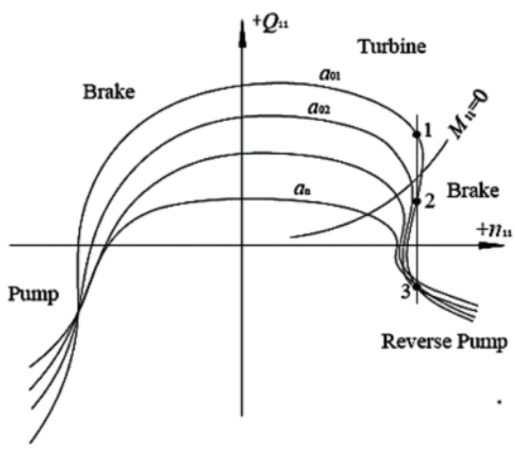


Fig. 1 Four quadrant characteristics of pump turbine on flow-speed curve[3]

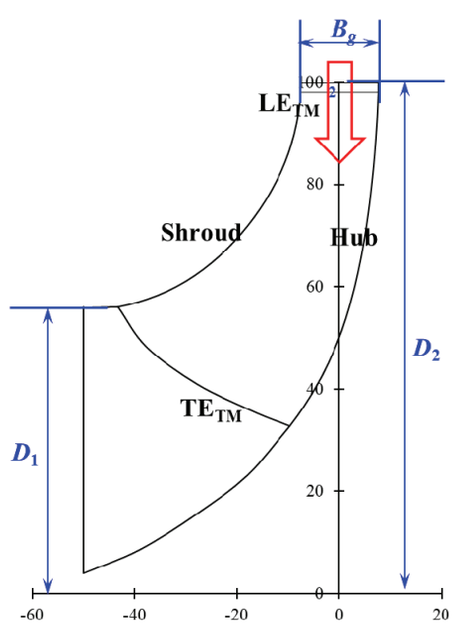


Fig. 2 Meridional shape of pump turbine in turbine mode

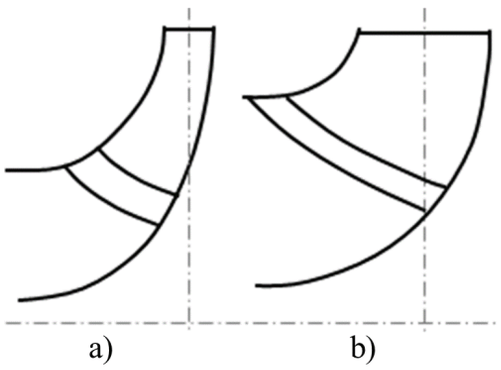


Fig. 3 Meridional shape of pump turbine according to specific speed a) $N_S$=30 and b) $N_S$=55

Generally, the pump turbine specific speed ranges from 30 to 55 [min$^{-1}$, m$^3$/s, m] according to pump mode. In the present study, the low and high specific speed pump turbines are selected to compare the S-Curve region accordingly. Fig. 2 shows the pump turbine meridional shape with basic dimensions. The meridional shape of the pump turbine is dependent on specific speeds. Fig. 3 shows the variation in meridional plane shape according to the pump turbine specific speed. The value of $D_1$ and $B_g$ increases gradually with a high specific speed pump turbine. The design method for the pump turbine is based on the gradient of discharge variation to head variation from the previous studies[14,15]. The detailed design specification of the pump turbine is shown in Table 1.

## 2.2 Numerical Methodology

The commercial code of ANSYS 2022R2[16] is used for the computational analysis of pump turbines in pump and turbine modes. ANSYS CFX 2022R2[16] uses Reynolds Averaged Navier Stokes (RANS) equations to solve the steady incompressible simulation. The hexahedral numerical grids are suitable for the proper and stable CFD analysis. ANSYS ICEM 2022R2[16] is used to create the hexahedral numerical grids with a $y^+ < 10$. Fig. 4 shows the numerical grids of the pump turbine model with each component.

Table 1 Design parameters of pump turbine

| Parameter | $N_S$=30 | $N_S$=55 |
|---|---|---|
| Head, $H_P$ | 410 m | 355 m |
| Flow rate, $Q_P$ | 84 m$^3$/s | 101 m$^3$/s |
| Rotational speed, $N$ | 300 min$^{-1}$ | 450 min$^{-1}$ |
| Output Power, $P_T$ | 350 MW | 450 MW |
| Input Power, $P_P$ | 360 MW | 410 MW |
| Diameter ratio, $D_2/D_1$ | 1.96 | 1.28 |
| Width ratio, $B_g/D_1$ | 0.12 | 0.22 |
| Number of Impeller Blades | 9 | 9 |
| Number of Guide Vanes | 20 | 20 |
| Blade angle at $LE_{TM}$ | 21° | 21° |

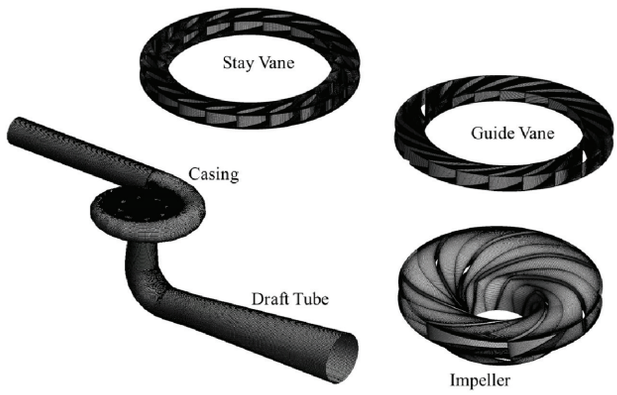


Fig. 4 Numerical grids of $N_S$=30 pump turbine model

The mesh dependency test is conducted to select a suitable mesh number for CFD analysis. Grid convergence test was carried out with three grid densities ($G_1$, $G_2$, $G_3$) using grid convergence index($GCI$) method[17] and pump efficiency ($\eta$) was chosen for sensitivity study. The $GCI$ is computed using Eq. (3).

$$GCI_{fine}^{21} = \frac{1.25\epsilon_a^{21}}{r_{21}^{p_0}-1} \tag{3}$$

Table 2 Discretization error for the numerical solution

| | $N_S$=30 | $N_S$=55 |
|---|---|---|
| $G_1$, $G_2$, $G_3$ | 13.1×10$^6$, 6.7×10$^6$, 4.3×10$^6$ | |
| $r_{21}$ | 1.26 | |
| $r_{32}$ | 1.15 | |
| $\eta_1$ | 92.85 | 92.79 |
| $\eta_2$ | 93.20 | 92.89 |
| $\eta_3$ | 93.10 | 92.91 |
| $p_0$ | 4.36 | 5.28 |
| $\eta_{ext}^{21}$ | 92.71 | 92.68 |
| $\epsilon_a^{21}$ | 0.0038 | 0.0020 |
| $\epsilon_{ext}^{21}$ | 0.0015 | 0.0012 |
| $GCI_{fine}^{21}$ | 0.19% | 0.15% |
| $GCI_{fine}^{32}$ | 0.01% | 0.01% |

where $G$ is grid number, $\eta$ is pump efficiency, $\epsilon$ is the relative error, $r$ is grid refinement factor, $p_0$ is apparent order of numerical solution, the subscript $a$ and $ext$ are approximate and extrapolated relative error values, respectively.

Table 2 shows the discretization error for the numerical solution. The $GCI$ is less than 1% for $N_S$=30 and 55 pump turbine. Fig. 4 shows the mesh dependency test for the $N_S$=30 pump turbine CFD analysis at $Q/Q_{BEP}$=1.00. Fig. 5 indicates that a 6.7 million node number will be suitable for CFD analysis of the pump turbine. The boundary conditions for CFD analysis of the pump turbine are shown in Table 3. In turbine mode, the inlet and outlet boundary conditions are total pressure and static pressure of 1 atm, respectively[18]. In turbine mode, the guide vane opening controls the flow rate. The boundary conditions for pump mode are static pressure and mass flow rate for the inlet and outlet, respectively. In addition, CFD analysis on the S-Curve region is conducted using total pressure inlet and mass flow rate outlet. The turbine mode operates at the same guide vane opening, but the flow rate is reduced to obtain the S-Curve region in the pump turbine.

Furthermore, the RANS equation with the shear stress transport (SST) turbulence model is selected for CFD analysis in pump and turbine modes. The SST shows a better prediction of low separation under reverse pressure gradients[19]. The whole domain analysis is employed, and a frozen rotor interface is selected between stationary and rotating components. The no-slip wall conditions are specified for the CFD analysis. The high-resolution and advection schemes are chosen for the proper CFD analysis. The residual root mean square value for the convergence criteria is $10^{-6}$ for all the governing equations.

Table 3 Boundary conditions for pump turbine analysis

| Specification | Turbine | Pump |
|---|---|---|
| Inlet | Total Pressure | Static Pressure |
| Outlet | Static Pressure | Mass Flow Rate |
| Turbulence Model | Shear Stress Transport | |
| Interface Model | Frozen Rotor (Steady State) | |
| Reference Pressure | 1 atm | |
| Wall Condition | No Slip Wall | |

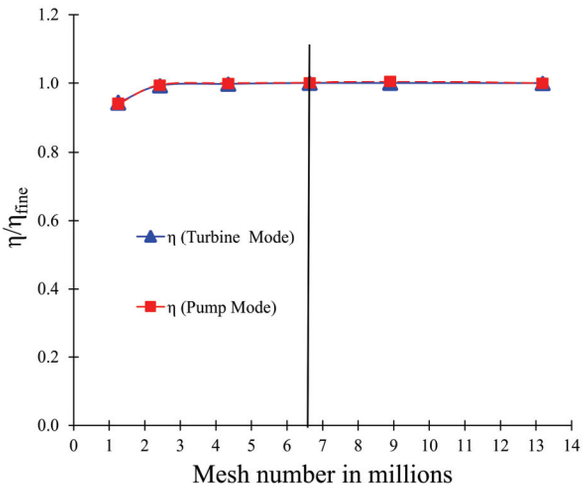


Fig. 5 Mesh dependency test for $N_S$=30 pump turbine at $Q/Q_{BEP}$=1.00

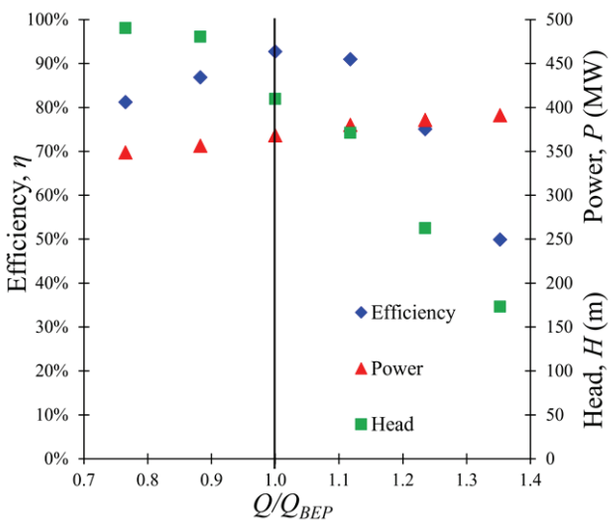


Fig. 6 Performance curves of pump turbine $N_S$=30 in pump mode

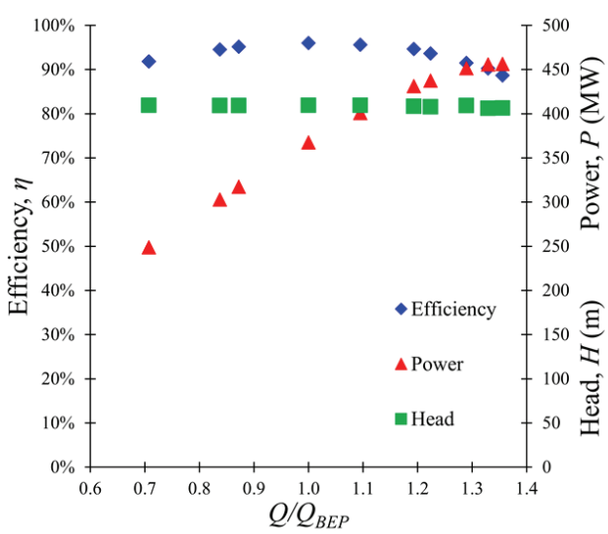


Fig. 7 Performance curves of pump turbine $N_S$=30 in turbine mode

## 3. Results and Discussion

### 3.1 Performance curves of pump turbine

Fig. 6 shows the $N_S$=30 pump turbine performance curves in pump mode. The best efficiency of the pump turbine is 93% in pump mode, which matches the design point. It confirms that the design process of the pump turbine is acceptable. $N_S$=30 pump turbine head reaches 490 m at $Q/Q_{BEP}$=0.75. Fig. 7 shows the performance curves of $N_S$=30 pump turbine in turbine mode. The performance curves in turbine mode are generated by changing the guide vane opening, which controls the flow rate. The best efficiency of $N_S$=30 pump turbine in turbine mode is 96%. The performance of $N_S$=30 pump turbine in turbine mode is consistent at partial and high flow rates. The efficiency is above 90% from $Q/Q_{BEP}$= 0.70 to 1.30. The output power of the pump turbine in turbine mode reaches above 450 MW with 90% efficiency at $Q/Q_{BEP}$=1.30. It implies that the design of $N_S$=30 pump turbine is acceptable to operate in both pump and turbine modes.

The performance curves of $N_S$=55 pump turbine in pump and turbine modes are shown in Figs. 8 and 9, respectively. The best efficiency of $N_S$=55 pump turbine in pump mode is 93% at design operating conditions. In turbine mode, the $N_S$=55 pump turbine's best efficiency is 93%. The efficiency of $N_S$=55 pump turbine from $Q/Q_{BEP}$=0.70 to 1.30 is above 90%, which suggests the wide range of operation of the pump turbine in turbine mode. $N_S$=55 pump turbine can also generate a maximum output power of 600MW when it operates at $Q/Q_{BEP}$=1.25. The low and the high specific speed pump turbines generate immense output power compared to the input power required to operate in pump mode.

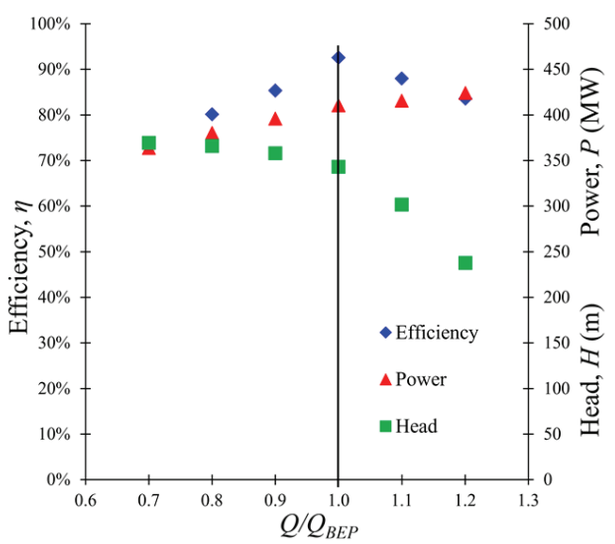


Fig. 8 Performance curves of pump turbine $N_S$=55 in pump mode

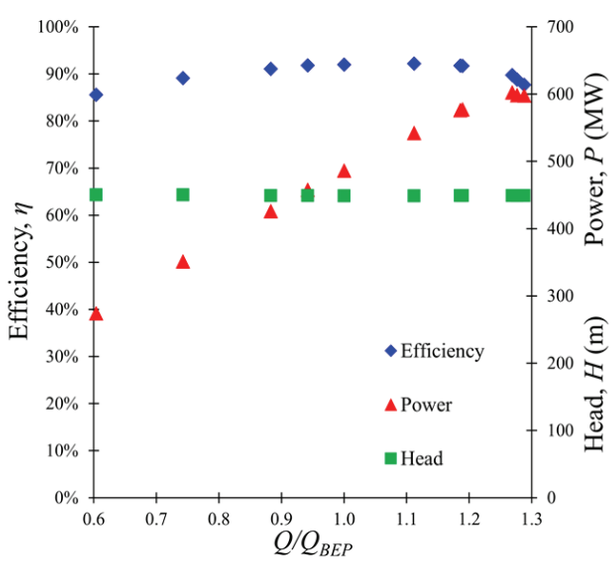


Fig. 9 Performance curves of pump turbine $N_S$=55 in turbine mode

### 3.2 Internal flow of pump turbine in turbine mode

The internal flow of $N_S$=30 pump turbine at various flow conditions helps to understand the flow behavior of the pump turbine. Fig. 10 shows the pressure contours in $N_S$=30 pump turbine at various flow conditions in turbine mode. At the $Q/Q_{BEP}$=0.75, the pressure at the impeller outlet is lower than $Q/Q_{BEP}$=1.00 and 1.30, respectively. Fig. 11 indicates the velocity vector distribution in the impeller cross-section in turbine mode. At $Q/Q_{BEP}$=0.75, the

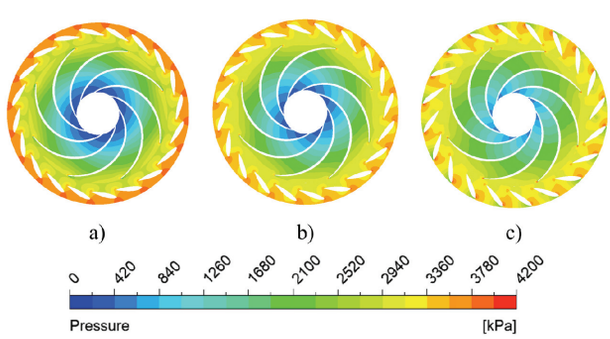


Fig. 10 Pressure contours of $N_S$=30 pump turbine in turbine mode at a) $Q/Q_{BEP}$=0.75, b) $Q/Q_{BEP}$=1.00 and c) $Q/Q_{BEP}$=1.30

quantity of velocity vectors at the impeller inlet is highly concentrated compared to $Q/Q_{BEP}$=1.00 and 1.30, respectively. At $Q/Q_{BEP}$=1.30, the impeller inlet velocity vectors are comparatively higher and distributed evenly than $Q/Q_{BEP}$=0.75 and 1.00. It suggests that at partial flow conditions, the flow behavior at the impeller inlet in turbine mode is concentrated and contributes to shock loss.

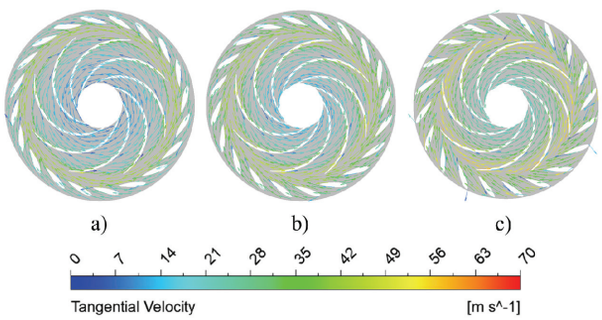


Fig. 11 Velocity vectors of $N_S$=30 pump turbine in turbine mode at a) $Q/Q_{BEP}$=0.75, b) $Q/Q_{BEP}$=1.00 and c) $Q/Q_{BEP}$=1.30

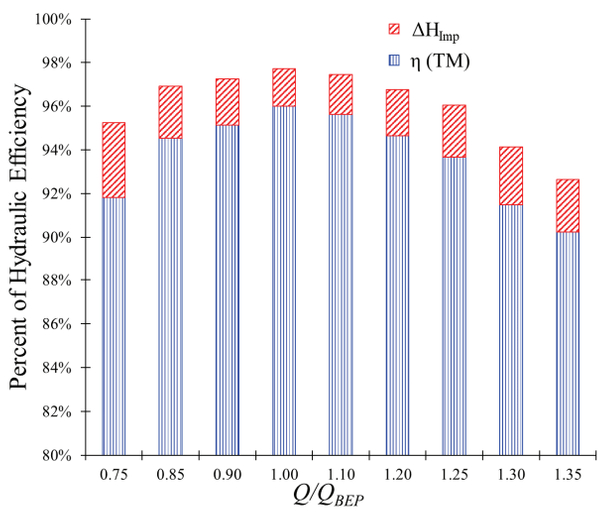


Fig. 12 Efficiency and hydraulic loss in impeller of $N_S$=30 pump turbine in turbine mode (TM)

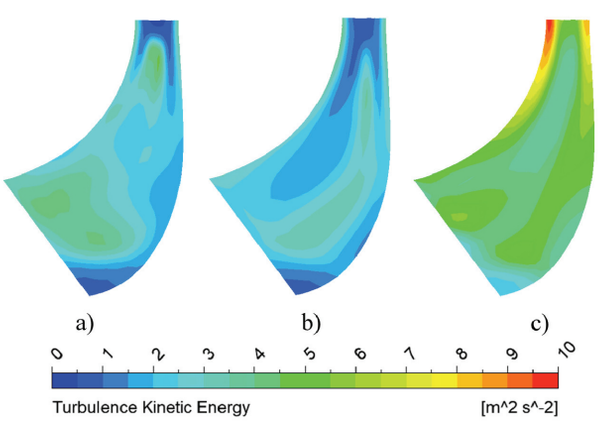


Fig. 13 Turbulence kinetic energy of $N_S$=30 pump turbine in turbine mode at a) $Q/Q_{BEP}$=0.75, b) $Q/Q_{BEP}$=1.00 and c) $Q/Q_{BEP}$=1.30

The impeller head loss in turbine mode is calculated using Eq. (4).

$$\Delta H_{Imp} = \frac{\Delta p_{Imp} - \frac{T\omega}{Q}}{\rho g H} \tag{4}$$

where $\Delta H_{Imp}$ is a hydraulic loss in the impeller, $\Delta p_{Imp}$ is the pressure difference in impeller (Pa), $T$ is the output torque of impeller (Nm), $\omega$ is rotational speed (rad/s), $\rho$ is water density (kg/m³), $g$ is the acceleration due to gravity (m/s²), and $H$ is the effective head (m).

Fig. 12 shows the impeller head loss in turbine mode of $N_S$=30 pump turbine. The impeller head loss is minimum at $Q/Q_{BEP}$=1.00. It implies that the impeller head loss is high at off-design operating conditions. The impeller head losses are 3.5%, 1.8%, and 2.7% of hydraulic efficiency in the turbine mode of $N_S$=30 pump turbine at $Q/Q_{BEP}$=0.75, 1.00 and 1.30, respectively.

Fig. 13 shows the average turbulence kinetic energy distribution in the $N_S$=30 pump turbine impeller meridional shape. The turbulence kinetic energy (TKE) explains the mean kinetic energy per unit masses associated with eddies in turbulent flow and quantifies the fluctuations in velocity caused by eddies and vortices. The TKE amount in meridional flow passage at $Q/Q_{BEP}$=1.00 is lower than $Q/Q_{BEP}$=0.75 and 1.30, which suggests that at the best efficiency point, the average velocity fluctuation is low compared to partial and high flow conditions. Hence, the eddies and vortices quantities are minimal at $Q/Q_{BEP}$=1.00.

### 3.3 S-Curve analysis for pump turbine

The hydraulic losses in the turbine mode at partial flow rates induce an S-Curve region in the pump turbine. The S-Curve region occurs in the turbine mode when the speed-flow curves have a positive slope[20]. The present study examined S-Curve behavior in low and high specific pump turbines. The S-Curve nature is explained using the meridian and the circumferential velocity coefficients[5]. Meridian and

circumferential velocity coefficients are shown in Eqs. (5) and (6), respectively.

$$k_{m_1} = \frac{Q}{\pi D_2 B_g \sqrt{2gH}} \tag{5}$$

$$\phi_1 = \frac{\pi D_2 N}{60\sqrt{2gH}} \tag{6}$$

where $N$, $Q$, $H$, and $P$ are rotational speed ($min^{-1}$), flow rate ($m^3/s$), effective head (m), and output power (kW). $D_2$ and $B_g$ are the larger diameter and width of the pump turbine in turbine mode, respectively, as shown in Fig. 2. $g$ is the acceleration due to gravity ($m/s^2$). $k_{m_1}$ and $\phi_1$ are meridian and circumferential velocity coefficients, respectively.

Fig. 14 shows the S-Curve of $N_S$=30 pump turbine with meridian and circumferential velocity coefficients. The $N_S$=30 pump turbine shows the proper operation in turbine mode from $\phi_1$=0.74 to 1.28 and $k_{m_1}$=0.16 to 0.09, respectively. The S-Curve region appears from $\phi$=1.31 and $k_{m_1}$=0.07 in $N_S$=30 pump turbine, with steep inclination. The detailed analysis of the S-Curve region showed that the S-Curve region appears when the partial flow rate reaches below 50% in turbine mode.

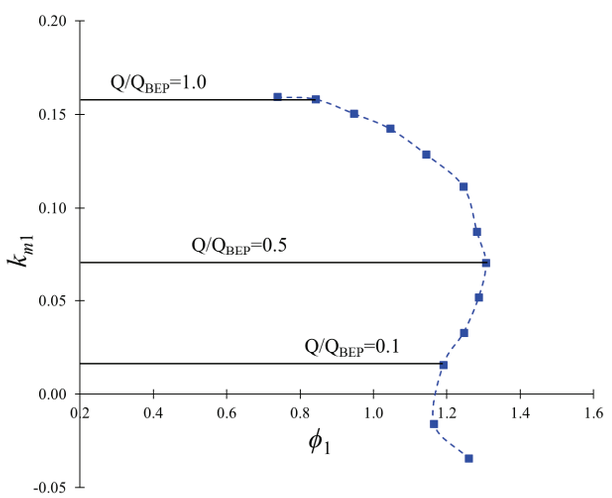


Fig. 14 S-Curve of $N_S$=30 pump turbine in turbine mode at guide vane opening of 22°

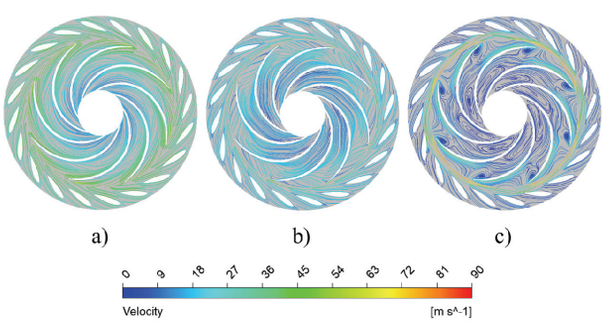


Fig. 15 Velocity streamlines of $N_S$=30 pump turbine in S-Curve region at a) $Q/Q_{BEP}$=1.00, b) $Q/Q_{BEP}$=0.50 and c) $Q/Q_{BEP}$=0.10

Fig. 15 indicates the streamline distribution in the S-Curve region. At $Q/Q_{BEP}$=1.00, velocity streamlines show smooth distribution. When the flow rate decreases, the velocity streamlines indicate the vortices and eddies in the impeller flow passage. At $Q/Q_{BEP}$=0.50, the velocity streamlines show a slight deviation in the impeller flow passage. A significant amount of eddies and vortices occur in the impeller flow passage when the pump turbine operates at $Q/Q_{BEP}$=0.10. The vortices and eddies are visible at the impeller inlet in turbine mode. The velocity magnitude is very high at the interface between the guide vane and impeller, which behaves as flow restriction in impeller flow passage and induces the eddies and vortices.

Fig. 16 shows the radial velocity distribution at the interface between the guide vane and impeller in

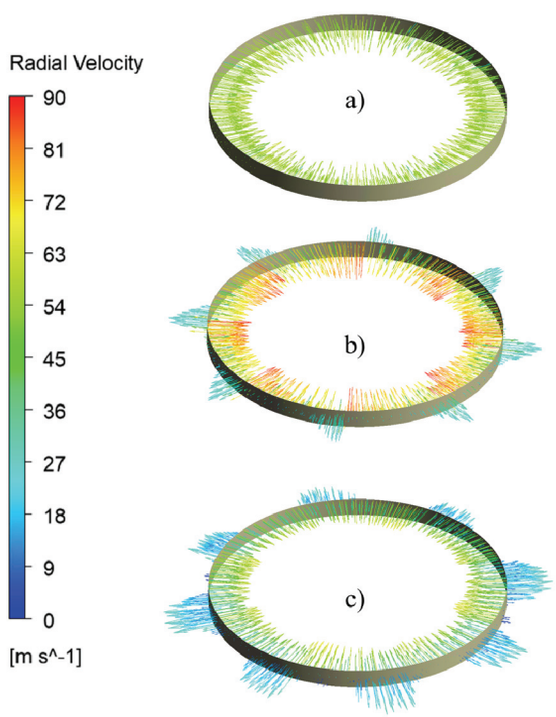


Fig. 16 Radial velocity vectors in S-Curve of $N_S$=30 pump turbine at interface between guide vane and impeller a) $Q/Q_{BEP}$=1.00, b) $Q/Q_{BEP}$=0.50 and c) $Q/Q_{BEP}$=0.10

turbine mode. At $Q/Q_{BEP}$=1.00, the radial velocity is directed towards the impeller and indicates the smooth flow behavior without any eddies and vortices. When the radial velocity direction changes, it causes eddies and vortices in the impeller flow passage. In the S–Curve region at $Q/Q_{BEP}$=0.50 and 0.10, the radial velocity is in inward and outward directions, which increases the intensity of secondary flow and eddies.

Fig. 17 shows the S–Curve of $N_S$=55 pump turbine with various flow rates. In a high specific speed pump turbine, $\phi_1$ and $k_{m_1}$ values are higher and lower than in a low specific speed pump turbine, respectively. In $N_S$= 55 pump turbine, the turbine mode operates from $\phi_1$= 0.68 to 1.49 and $k_{m_1}$= 0.16 to 0.08. The S–Curve region for $N_S$=55 pump turbine is from $\phi_1$=1.50 and $k_{m_1}$=0.06. Fig. 18 shows the velocity streamlines in the impeller cross–section view in turbine mode. At $Q/Q_{BEP}$=1.00, the velocity streamlines show uniform distribution with an average velocity of 45 m/s. At $Q/Q_{BEP}$=0.50, a slight deviation in the velocity streamlines appears at the blade wall, but the high–velocity flow is observed at the leading edge of the impeller in turbine mode. The S–Curve region at $Q/Q_{BEP}$=0.10 shows secondary flow in the impeller flow passage. The high–magnitude velocity streamlines are observed at the guide vane and impeller interface.

Fig. 19 shows the radial velocity vectors at the interface between the guide vane and the impeller. At $Q/Q_{BEP}$=1.00, the 45 m/s magnitude of radial velocity is directed toward the impeller. It suggests that radial velocity has uniform magnitude and direction at best operating conditions in turbine mode. Fig. 19 indicates that at $Q/Q_{BEP}$=0.50, the magnitude of radial velocity is variable and directed towards the impeller. The quantity of radial velocity outward of the impeller is minimum, which implies the minimum secondary flow at a partial flow rate. At $Q/Q_{BEP}$=0.10, the radial velocity vectors are directed outward, which causes recirculation and eddies flow in the impeller flow

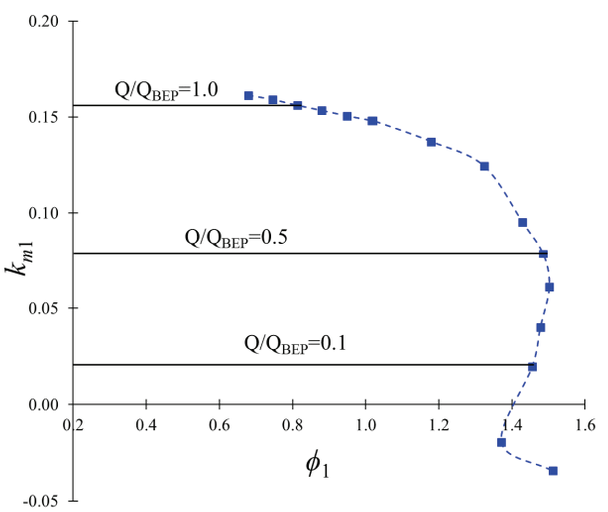


Fig. 17 S–Curve of $N_S$=55 pump turbine in turbine mode at guide vane opening of 22°

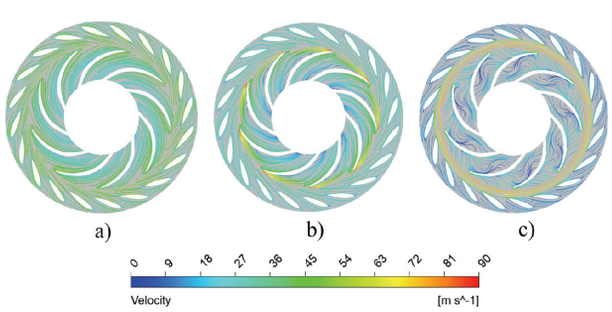


Fig. 18 Velocity streamlines of $N_S$=55 pump turbine in S–Curve region at a) $Q/Q_{BEP}$=1.00, b) $Q/Q_{BEP}$=0.50 and c) $Q/Q_{BEP}$=0.10

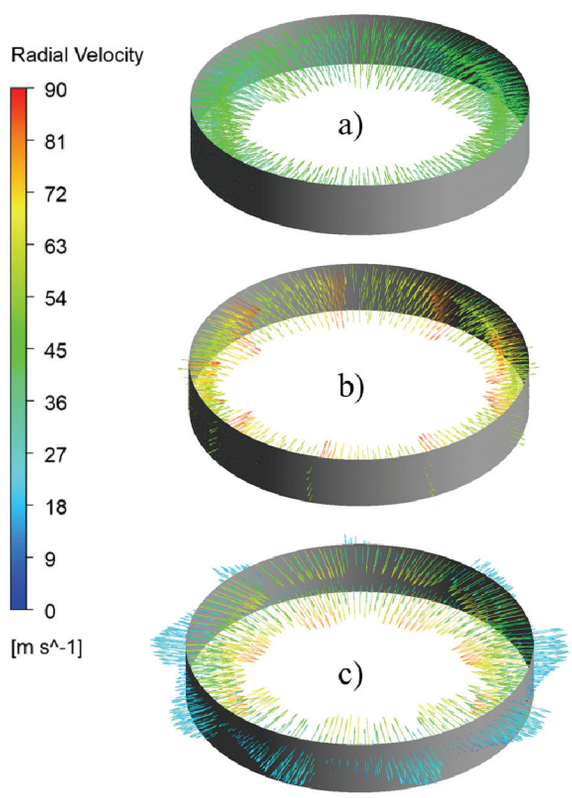


Fig. 19 Radial velocity vectors in S–Curve of $N_S$=55 pump turbine at interface between guide vane and impeller a) $Q/Q_{BEP}$=1.00, b) $Q/Q_{BEP}$=0.50 and c) $Q/Q_{BEP}$=0.10

passage. It implies that the number of eddies, vortices, and secondary flow is higher in the S-Curve region.

The comparison of turbulence kinetic energy (TKE) of $N_S$=55 pump turbine in the S-Curve region is shown in Fig. 20. The TKE indicates the magnitude of velocity fluctuation and eddies in the impeller flow passage. At $Q/Q_{BEP}$=1.00, the magnitude of TKE is approximately zero throughout the impeller flow passage, which implies no velocity fluctuations in the impeller. At a partial flow rate, TKE tends to increase drastically in the impeller flow passage. At $Q/Q_{BEP}$=0.50, the TKE magnitude is below 35 m²/s². Furthermore, the TKE magnitude is more than 120 m²/s² at the impeller in turbine mode. It concludes that the velocity fluctuation, eddies, and vortex intensity increase drastically at $Q/Q_{BEP}$=0.10.

Fig. 21 shows the pressure distribution at the interface between the guide vane and impeller in turbine mode. The normalized pressure is used to compare the pressure fluctuation at the impeller inlet in S-Curve region. The normalized pressure is calculated using Eq. (7).

$$p_{norm} = \frac{p}{\rho g H} \tag{7}$$

where $p_{norm}$ is normalized pressure, $p$ is static pressure (Pa), $\rho$ is water density (kg/m³), $g$ is acceleration due to gravity (m/s²), and $H$ is the effective head (m).

At $Q/Q_{BEP}$=0.50 and impeller inlet in the S-Curve region, the pressure fluctuation in $N_S$=30 is two times higher than that of $N_S$=55 pump turbine. The high specific pump turbine has lower pressure fluctuation at the impeller inlet in the S-Curve region. Fig. 22 shows the S-Curve comparison between $N_S$=30 and 55 pump turbines at 22° guide vane opening. The meridian and circumferential velocity coefficients for $N_S$=30 and 55 pump turbines are approximately identical at $Q/Q_{BEP}$=1.00. The inception and ending points of the S-Curve region for $N_S$=30 and 55 pump turbines are $\phi_1$=1.31 to 1.17 and 1.50 to 1.40, respectively. The inclination angle of the S-Curve for $N_S$=30 is higher than $N_S$=55 pump turbines. The S-Curve slope for $N_s$=30 and 55 are 27° and 22°, respectively. It concludes that the S-Curve of low-specific speed pump turbines is steeper than that of high-specific speed pump turbines.

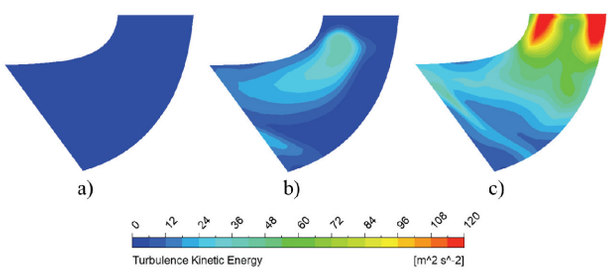


Fig. 20 Turbulence kinetic energy of $N_S$=55 pump turbine in S-Curve region at a) $Q/Q_{BEP}$=1.00, b) $Q/Q_{BEP}$=0.50 and c) $Q/Q_{BEP}$=0.10

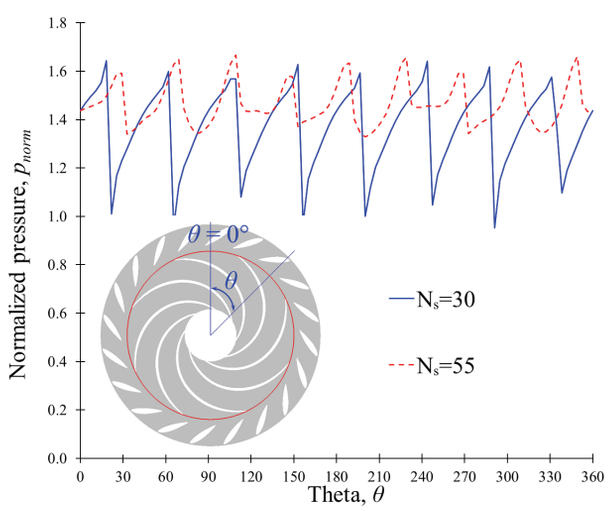


Fig. 21 Pressure distribution at impeller inlet in the S-Curve region of $N_S$=30 and 55 pump turbine at $Q/Q_{BEP}$=0.50

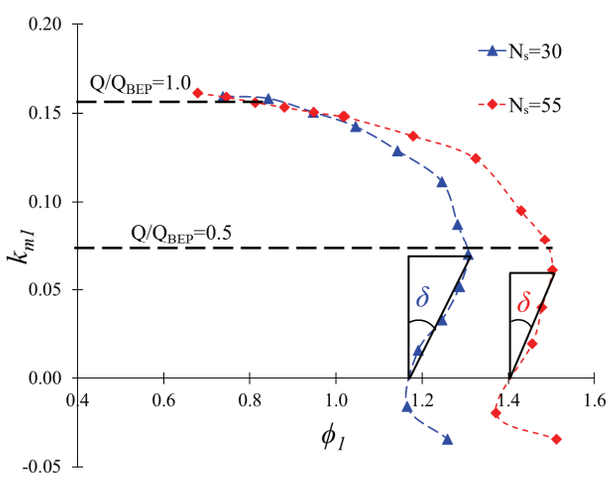


Fig. 22 Comparison between $N_S$=30 and 55 pump turbine S-Curve in turbine mode at guide vane opening of 22°

## 4. Conclusion

The pump turbines with various specific speeds with the same blade angles were selected for comparative study. The pump turbine impeller geometry changes drastically with a specific speed. The diameter and width ratios differ with the change in the pump turbine specific speed. The low-specific speed pump turbine shows better hydraulic performance in turbine mode than the high specific speed pump turbine at normal operating conditions. In pump mode, low and high specific speed pump turbines showed an efficiency of 93% at best operating conditions. The pump turbine's specific speed significantly influences the turbine's performance. $N_S$=30 and 55 pump turbines achieved 96% and 93% efficiency in turbine mode, respectively.

The S-Curve behavior is impacted by the pump turbine specific speed. At a low specific speed pump turbine, the S-Curve is steeper compared to a high specific speed pump turbine. The S-Curve phenomenon is more significant at $N_S$=30 than $N_S$=55 pump turbine. $N_S$=30 pump turbine shows significant eddies and secondary vortex in the S-Curve region compared to $N_S$=55 pump turbine at partial flow conditions. At the S-Curve region and $Q/Q_{BEP}$=0.50, $N_S$=55 pump turbine shows that the radial velocity vectors are directed towards the impeller compared to $N_S$=30 pump turbine. Hence, the S-Curve for the low-specific pump turbines is steeper than the high-specific speed pump turbines.

It would be instructive to perform the dynamic analysis in the S-Curve region for future works. More studies focused on the design of pump turbines, which will be applicable for variable speed operation.

## References


(1) Rehman, S., Al-Hadhrami, L.M. and Mahbub, A.M., 2015, "Pumped hydro energy storage system: a technological review," Renewable Sustainable Energy Reviews, Vol. 44, pp. 586-598.

(2) Nautiyal, H. and Varun, A. K., 2010, "Reverse running pumps analytical, experimental and computational study: a review," Renewable Sustainable Energy Reviews, Vol. 14, No. 7, pp 2059–2067.

(3) Amblard, H., Henry, P., Borciani, G., Martin, G., Guiton, P. and Thalmann, R., 1985, "Behavior of Francis turbines and pump-turbines at partial flow," La Houille Blanc, Vol.5, pp 435–40.

(4) Pérez-Díaz, J. I., Cavazzini, G., Blázquez, F., Platero, C., Fraile-Ardanuy, J. and Sánchez, J. A., 2014, "Technological developments for pumped-hydro energy storage, Technical Report. Mechanical Storage Subprogramme," Joint Programme on Energy Storage, European Energy Research Alliance.

(5) Xia, L., Cheng, Y., You, J., Zhang, X., Yang, J. and Qian, Z., 2017, "Mechanism of the S-shaped characteristics and the runaway instability of pump-turbines," Journal of Fluids Engineering, Vol. 139, No. 3, pp. 031101.

(6) Pejovic, S. and Karney, B., 2014, "Guidelines for transients are in need of revision," IOP Conference Series: Earth and Environmental Science, Vol. 22, pp. 042006.

(7) Nicolet, C., Alligné, S., Kawkabani, B., Koutnik, J., Simond, J. and Avellan, F., 2009, "Stability study of Francis pump-turbine at runaway," In: Proceedings of the 3rd international meeting of the workgroup on cavitation and dynamic problems in hydraulic machinery and systems,: Brno, Czech Republic.

(8) Hasmatuchi, V., Roth, S., Botero, F., Avellan, F. and Farhat, M., 2010, "High-speed flow visualization in a pump-turbine under off-design operating conditions," IOP Conference Series: Earth and Environmental Science, Vol. 12, pp. 012059.

(9) Hasmatuchi, V., Farhat, M., Roth, S., Botero, F. and Avellan, F., 2011, "Experimental evidence of rotating stall in a pump-turbine at off-design conditions in generating mode," Journal of Fluids Engineering, Vol. 133, No. 5, pp 051104

(10) Guggenberger, M., Senn, F., Schiffer, J., Jaberg, H., Gentner, C., Sallaberger, M. and Widmer, C., 2013, "Experimental investigation of the turbine instability of a pump turbine during synchronization," IOP Conference Series: Earth and Environmental Science, Vol. 22, No. 3, pp. 032015.

(11) Guggenberger, M., Senn, F., Schiffer, J., Jaberg, H., Sallaberger, M. and Widmer, C., 2015, "Investigating the dynamic aspects of the turbine instability of a pump turbine model," In: Proceedings of the 6th IAHR international meeting of the working group on cavitation and dynamic problems in hydraulic machinery and systems, Ljubljana, Slovenia.

(12) Staubli, T., Senn, F. and Sallaberger, M., 2008, "Instability of pump-turbines during start-up in the turbine mode," Hydro 2008, pp. 6-8.

(13) Yin, J., Wang, D., Wei, X., & Wang, L. (2013). Hydraulic improvement to eliminate S-shaped curve in pump turbine. Journal of Fluids Engineering, 135(7), 071105.

(14) Kubota, T., 1997, "Hydraulic Design of Francis Pump Turbine," in Hydraulic Design of Hydraulic Machinery, Ashgate Publishing Limited, Wiltshire, pp 465-484.
(15) Shrestha, U., Singh, P. M. and Choi, Y-D., 2019, "Design and Experimental Analysis on 3kW class Pump Turbine Model for Renewable ESS," KSFM, Vol. 22, No. 4, pp. 19-28.
(16) ANSYS Inc., 2022, "ANSYS CFX documentation ver 2022R2", http://www.ansys.com.
(17) Celik, I. B., Ghia, U., Roache, P. J., Freitas, C. J., Coleman, H. and Raad, P. E., 2008, "Procedure for Estimation and Reporting of Uncertainty Due to Discretization in CFD Applications," Journal of Fluids Engineering, Vol. 130, No. 7, pp. 078001.
(18) Shrestha, U. and Choi, Y-D., 2020, "A CFD-based shape design optimization process of fixed flow passages in a Francis hydro turbine," Processes, Vol. 8, No. 11, pp. 1392.
(19) Shrestha, U. and Choi, Y-D., 2022, "Estimation of Reverse Flow Rate in J-Groove Channel of AJP and SCP Models Using CFD Analysis," Processes, Vol. 10, No. 4, pp. 785.
(20) Gentner, C., Sallaberger, M., Widmer, C., Braun, O. and Staubli, T., 2012, "Numerical and experimental analysis of instability phenomena in pump turbines," IOP conference series: earth and environmental science. Vol. 15, No. 3, p. 032042.